Diagnosis of the surface layer damage in a 1960s reinforced concrete building

Case Studies in Construction Materials 1 (2014) 77–82

Contents lists available at ScienceDirect

Case Studies in Construction Materials

journal homepage: www.elsevier.com/locate/cscm

Case Study

Diagnosis of the surface layer damage in a 1960s reinforced concrete building

S.L. Pagliolico [a,*], R. Doglione [b], J.-M. Tulliani [a]

[a] Politecnico di Torino, Department of Applied Science and Technology, C. so Duca degli Abruzzi 24, 10129 Torino, Italy
[b] INSTM, Via G. Giusti 9, 50121 Firenze, Italy

ARTICLE INFO

Article history:
Received 22 November 2013
Received in revised form 17 April 2014
Accepted 20 April 2014
Available online 9 May 2014

Keywords:
Carbonation
Concrete
Corrosion
Bricks
Efflorescences
Black crusts

ABSTRACT

This work aimed to determine the degradation causes of the Palace of Public Works located in S. Giovanni square in Turin (Piedmont, Italy). The samples collected from the surface layer were characterized by means of scanning electron microscopy (SEM), X-ray diffraction (XRD), thermogravimetric coupled with differential thermal analysis (TG-DTA), mercury intrusion porosimetry measurements (MIP) and phenolphthalein test. Metallographic and elemental analyses were also carried out on the steel reinforcing bars. An exhaustive picture of the main causes of deterioration was drawn in order to design the intervention of rehabilitation.

1. Introduction

The project of the architects Garbaccio, Passanti and Perona won in 1956 the second prize of the "Competition for the preliminary design work on the offices of Public Works of the Turin City located in Piazza S. Giovanni" (the first prize was not awarded) and was built in 1961. The "New Palace of Public Works in Turin" filled a void due to the demolition of the 17th century building of the Italian architect Amedeo di Castellamonte bombed during 2nd World War. The six floors building (23 m in height) consisted of a reinforced concrete structure with brick infill (Fig. 1(a–c)).

Direct exposure to weathering and air pollutants involved soon damage to concrete pilasters and facing bricks. During 42 years, numerous patches and repairs were carried out, without never facing the problem in depth. In 2004, the state of degradation of the Palace of Public Works was widespread throughout the building: it was considerable in the eastern and western façades and very marked in the northern elevation (Fig. 1, suppl. mat.), but was minor in the southern façade. Sometimes, concrete covers were easily removed manually (Fig. 1d and e) (sample 11 – Table 1). Steel reinforcing bars showed a variable state of corrosion, sometimes very pronounced, with a certain loss of structural integrity, while in other areas they were not corroded at all. Regarding facing bricks and brick laying mortar, the most diffuse degradations were lacunas, pulverization, delamination, cracking, presence of efflorescences, patina and black crusts, dissolution and leaching of mortar between brick courses and the presence of salts inside the masonry (Fig. 2, suppl. mat.).

* Corresponding author. Tel.: +39 0110904677.
E-mail address: simonetta.pagliolico@polito.it (S.L. Pagliolico).

http://dx.doi.org/10.1016/j.cscm.2014.04.006

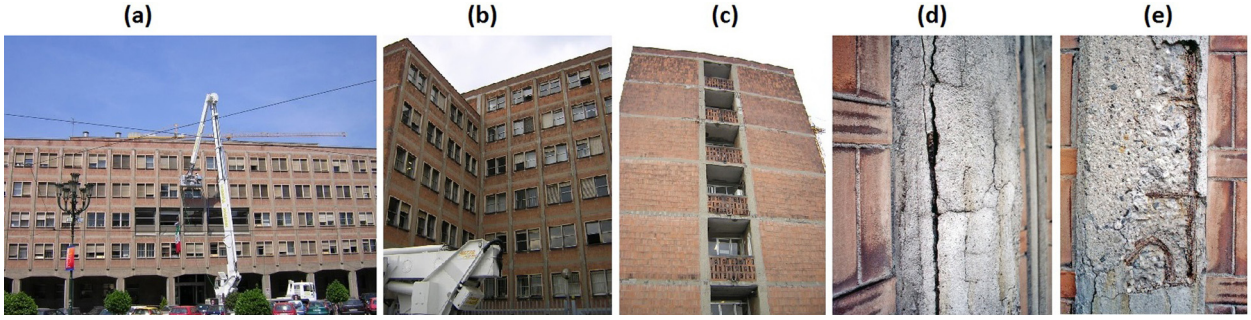

Fig. 1. Palace of Public Works in S. Giovanni square (Turin-Italy): eastern (a) and northern façades (b–e).

2. Materials and methods

More than 30 samples were investigated to determine the nature of concrete, mortars, bricks and steel reinforcing bars and of degradation products in view of a rehabilitation intervention (Table 1). Freshly cut cores of reinforced concrete were extracted by drilling for carbonation depth measurement. Samples of bricks and mortars were collected with a scalpel. Incoherent efflorescences were sampled by means of a brush from brick surface. Black crusts were removed with a bistouri.

Table 1
Visual analysis, sampling points, analysis planning.

Samples no.	Visual analysis Material/degradation	Diagnostic aim	Analysis planning					
			XRD	TG-DTA	MIP	CD	SEM	MM
Northern façade								
1	Mortar/intact	Reference	☑		☑			
2	Brick/pulverized	Degradation products	☑					
3	Brick/Efflorescence	Salts identification	☑	☑				
4	Steel RB (sample 8)/intact	RB corrosion						☑
5	Steel bracket (samples 8)/corroded	Corrosion						☑
Northern-East façade								
6	Original RC (plastered)/spalling	Carbonation	☑		☑	☑		
Northern façade								
7	Original RC pillar/intact	Carbonation	☑	☑	☑	☑		
8	Steel RB (sample 9)/oxidized	RB Corrosion						☑
9	Original RC beam/spalling	Carbonation	☑		☑	☑		
10	Mortar/degraded	Degradation products	☑		☑			
11	RC cover/spalling	Degradation products	☑		☑			
12	Mortar/pulverized	Degradation products	☑					
Western façade								
13	Original RC/spalling	Carbonation	☑		☑	☑		
14	Original concrete (plastered)/degraded	Carbonation	☑		☑	☑		
15	Original RC/spalling	Carbonation/RB corrosion	☑		☑	☑		☑
16	Brick/black crust	Degradation products	☑		☑		☑	
17	Efflorescence on brick	Salts identification	☑	☑				
18	Mortar/degraded	Degradation products	☑		☑			
Eastern façade								
19	Brick/intact	Reference	☑		☑			
20	Original concrete (plastered)/intact	Reference	☑		☑	☑		
21	Original concrete beam/intact	Carbonation	☑		☑	☑		
22	Concrete repair mortar (core 19)	Nature/degradation	☑					
23	Original concrete beam	Carbonation	☑		☑	☑		
24	RC/carbonated	Carbonation/RB corrosion	☑		☑	☑		
25	RC/carbonated	Carbonation/RB corrosion				☑		
26	RC/carbonated	Carbonation/RB corrosion				☑		
27	RC/carbonated	RB corrosion						
28	RC/carbonated	Carbonation/RB corrosion				☑		
29	RC/carbonated	Carbonation/RB corrosion	☑		☑	☑		☑
30	RC/carbonated	Carbonation/RB corrosion			☑	☑		
31	RC/carbonated	Carbonation/RB corrosion	☑		☑			☑

RC, reinforced concrete; RB, steel reinforcing bar; CD, carbonation depth measurement; MM, metallographic microscopy observations.

XRD patterns were recorded with a Philips PW 1710 diffractometer between 5° and 70° in 2θ, with a step width of 0.04° and 2.5 s data collection per step (Cu Kα radiation and graphite secondary monochromator). Concrete samples were first roughly crushed in an agate mortar with an agate pestle and the powders were sieved with steel meshes having apertures of 0.600 mm and of 0.105 mm. The retained fraction at 0.600 mm was considered to be mainly due to aggregates, while the passing fraction at 0.105 mm was used to determine the mineralogical composition of the binder. TG-DTA were performed in air, using a Netzsch STA 409 thermal analyzer, between 20 and 1100 °C, with a heating rate of 5 °C/min. The opened porosity and the pore size distribution of the samples were determined by MIP (Carlo Erba 2000 with macropore unit). Carbonation depth measurements were determined on freshly cut cores (often adjacent to superficial evidence of corrosion) sprayed with a pH indicator (phenolphthalein alcoholic solution). The metal reinforcements have been collected by core drilling in areas where visual analysis indicated a possible corrosion. Corroded reinforcement samples were subjected to conditioning cycles to assess the consistency and thickness of the oxides. Some fragments were embedded in acrylic resin, grinded with abrasive papers, polished with diamond paste and analyzed by the metallographic microscope Reichert MeF3.

Elemental analysis on the steel reinforcement was performed using the optical spectrometer SpectroLab S7.

SEM analysis was carried out in order to evaluate the morphological aspects of the black crusts (SEM/EDAX PEI PHILIPS-Quanta inspect 200 LV operated at 15 kV in an ultra-high vacuum).

3. Results and discussion

3.1. Reinforced concrete

TG-DTA and XRD analyses (Fig. 2) showed in all the samples the presence of calcite (CC), quartz (Q), feldspar (calcium plagioclase) (F), mica (M), serpentine (S), antigorite (A) and chlorite (Cl). The latter coming from aggregates (typical constituent of siliceous river sand), while calcite could have different origins: from aggregates, as cement filler, and from degradation process. Soluble carbonates were evidenced by dissolution of aggregates fraction in HCl. The binder was presumably Portland cement, as denoted by the presence of portlandite (CH) and of ettringite ($3CaO{\cdot}Al_2O_3{\cdot}3CaSO_4{\cdot}32H_2O$, AFt) reflections at 4.9 Å and at 2.57 Å, respectively. TG-DTA and XRD analyses also showed the presence of gypsum ($CaSO_4{\cdot}2H_2O$, G), and of calcium mono-carboaluminate hydrate ($C_3A{\cdot}CaCO_3{\cdot}11H_2O$, CAm). The characteristic reflection of mono-sulfoaluminate ($3CaO{\cdot}(Al,Fe)_2O_3{\cdot}CaSO_4{\cdot}12H_2O$, AFm) at 9.94 Å was not found.

Although calcium silicate hydrates (CSH) are the main phases of hydrated Portland cement, they cannot be fully detected by XRD, because of their low crystallinity and of the overlapping of their reflections with the aggregate ones at high scanning angles. However, the presence of hydrates of calcium aluminate such as ettringite (AFt) may be indicative of the presence of hardened Portland cement. When added to Portland cement, fine limestone reacts with aluminates (C_3A, C_4AH_{13}) in the presence of water to form calcium mono-carboaluminate hydrate (CAm) (Guemmadi et al., 2008; Voglis et al., 2005). Then, the presence of CAm is also a good evidence of hardened Portland cement mixed with limestone. XRD patterns evidenced a different degree of carbonation of the examined samples: the presence of accentuated characteristic reflections of calcite, associated to the absence or the low intensity of the calcium hydroxide reflections, confirmed the results obtained by phenolphthalein tests.

DTA analysis performed on core 7 indicated the presence of ettringite (endothermic peak at 141.8 °C), of calcium hydroxide (CH) (endothermic peak at 450 °C) and of calcite (endothermic peak at 746.2 °C) (Fig. 2(b)). The mass loss relative to the endothermic peak at 141.8 °C was relatively low (1.16%). These results confirmed XRD data.

The values of the total intruded porosity of concrete cores varied between 10% and 13% except for samples 13, 21 and 23 with a total porosity of about 15–18%. Pore size distribution resulted bimodal in some samples (20, 6, 7, 9, 13, 14, 21 and 23).

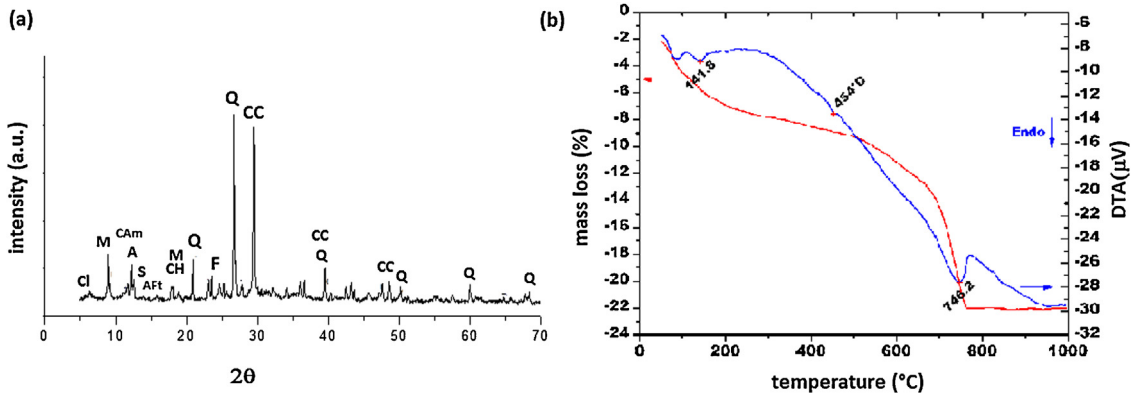

Fig. 2. Sample 7: (a) powder diffraction pattern: A = antigorite, AFt = ettringite, CAm = calcium mono-carboaluminate hydrate, CC = calcium carbonate (calcite), CH = calcium hydroxide, Cl = chlorite, F = feldspar, M = mica, Q = quartz, S = serpentine; (b) TG-DTA curves.

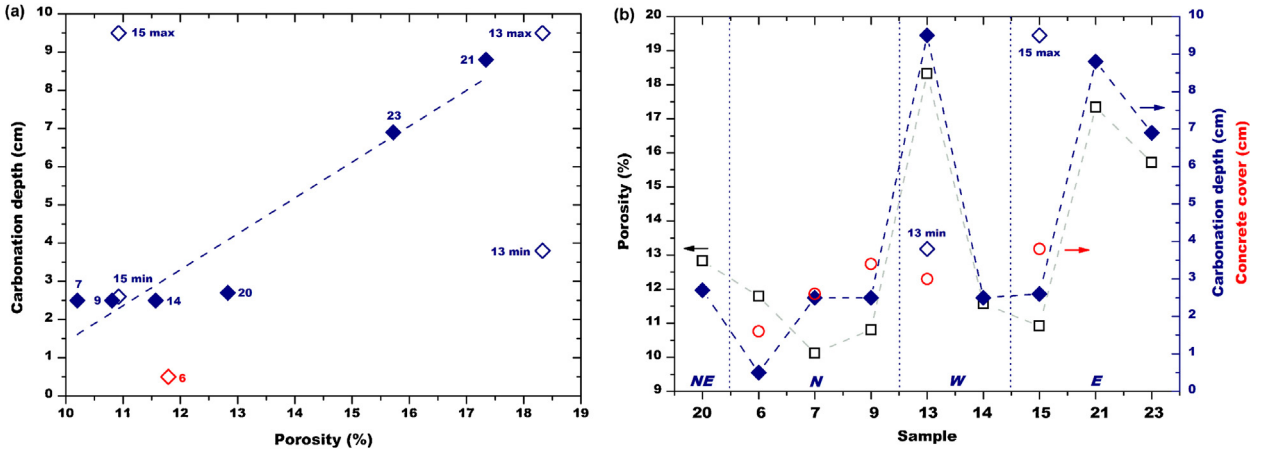

Fig. 3. (a) Carbonation depth versus total open porosity; (b) total open porosity, concrete cover thickness and depth of carbonation versus sampling point orientation.

The minimum average radius varied between 0.005 and 0.055 μm and the maximum average radius ranged between 0.2 and 0.3 μm. It is known in the literature that MIP does not give access to the total open porosity in mortars and concretes, however, the intruded pore volume may constitute a useful comparative index of concrete porosity (Diamond, 2000). Porosity depends on concrete mix-design (water/cement ratio, maximum size and size distribution of cement and aggregate particles), placing, compaction and curing operations which in turn determine the air entrapped inside hardened concrete and the degree of hydration of the cement paste. High values of open porosity are indicative of the concrete poor durability because porosity over 15% strongly influences permeability to external aggressive agents (Ye et al., 2006).

A variable carbonation depth was observed, depending on sampling points, on the presence of plastered coating made during maintenance operations (core 6) and of macro bubbles and cavities (cores 13 and 15) (Fig. 3, suppl. mat.). A maximum carbonation depth of 95–100 mm was recorded for samples, 13, 15 and 28 collected from western and eastern façades, respectively, while a minimum carbonation depth (5 mm) was recorded for sample 6, presumably due to the presence of a protective plastered coating of about 2 cm made during maintenance operations (Fig. 3c, suppl. mat.). A comparison between the trends of the carbonation depth and of the total intruded porosity pointed out a correlation between these parameters (Fig. 3(a)), except for core 6. Cores 15 and 13 showed a non-uniform depth of carbonation, for this reason the minimum and maximum values of carbonation depth were reported separately in Fig. 3(a) and (b), without calculating the average value. The measured thickness of concrete cover ranged between 2 and 4 cm (Fig. 3b). Some of these values are below the minimum value (3 cm) required by the current Eurocode N2 (EN, 2004), but this standard is more recent (1992) than the construction of the building.

CO_2 concentration in air should be around 280 ppm, while in polluted citizen sites it can reach the threshold value of 400 ppm (Yoon et al., 2007). Such a high CO_2 concentration threatens long-term durability of reinforced concrete structures by inducing carbonation/corrosion phenomena. As it is well known, in hardened concrete, reinforcing bars are protected against corrosion by passivation, due to the high alkaline pore water running up beyond 12.5. To activate the process of carbonation, the atmospheric CO_2 must first diffuse into concrete through pores and microcracks of the cement matrix, then must dissolve in water solution to form carbonate ions. The carbonate ions react with Ca^{2+} ions of the pore water solution forming calcium carbonate. The concentration of Ca^{2+} decreases and causes the dissolution of crystallized $Ca(OH)_2$. The solubility of calcium carbonate is much lower than that of calcium hydroxide, thus $Ca(OH)_2$ dissolves and $CaCO_3$ precipitates. The process continues until all $Ca(OH)_2$ is consumed and pH of the pore solution drops below 9 (Lagerblad, 2005).

The kinetic of carbonation is affected by relative humidity (Lagerblad, 2005): above 80% RH capillary pores on concrete surface are saturated with water so that CO_2 gas diffusion decreases, while below 50% RH, pore water evaporates and CO_2 gas cannot dissolve. The critical humidity range for high carbonation rate corresponds to moderately humid environments (exposure class XC3 by UNI EN206-1 (UNI EN, 2006)) and cyclic wet and dry conditions, such as external structures exposed to rain (exposure class XC4), which corresponds to the situation of the entire building. The active corrosion starts when the carbonation front is near the steel/concrete interface. Continued exposure of steel to oxidizing agents causes the formation of layers of iron oxides and hydroxides having different degree of oxidation, with a much lower density than that of iron. This causes a considerable increase in volume of the surface layer which generates sufficient stress to disrupt concrete cover by cracking and spalling. Furthermore, the porosity of the hydrated oxides does not guarantee any protection of the base metal allowing the corrosion to go on. Carbonation of the concrete starts from the outer surface layer and moves progressively inwards. Well known Eq. (1) describes the depth of carbonation as a function of time (Lagerblad, 2005; Gajda and MacGregor Miller, 2000; Ho and Lewis, 1987):

$$s = Kt^{0.5} \tag{1}$$

where s is the carbonated depth at time t, and K is the carbonated rate constant derived from Fick's first law.

Table 2
Chemical composition of steel rebars (mass%).

C	Si	Mn	P	S	Cr	Cu	Fe
0.24	0.44	0.61	0.053	0.084	0.25	0.41	Bal.

The carbonation rate constant K (mm/year$^{0.5}$) not only depends on environmental conditions: RH, temperature and carbon dioxide concentration, but also on concrete quality: water/cement ratio, degree of compaction and hydration, type and amount of cement, alkali content and basicity, and the presence of damaged zones and cracks (Pade and Guimaraes, 2007). K constant could vary between 0.5 and 157 mm/year$^{0.5}$, which corresponds to carbonation depths between 3.2 and 97.2 mm after 42 years of service life. The highest carbonation rate constants are observed in low compressive strength concrete (<15 MPa) exposed to high concentrations of CO_2 and moderate humidity (Ho and Lewis, 1987). K constant was calculated for samples 6, 7, 9, 11, 13, 14, 15, 20, 21 and 23 (Table 1, suppl. mat.): all the values exceed 3.7 mm/year$^{0.5}$, with the exception of sample 6. From visual analysis and by comparing these values with literature data it is possible to classify the concrete collected from the eastern, north-eastern, northern and western façades as sheltered/exposed (protected from direct rain by cover or overhang or outdoor exposed concrete), with compressive strength below 35 MPa (Lagerblad, 2005; Ho and Lewis, 1987). To conclude, the observed different porosity between cores 13, 15, 21, 23 and the other samples may be explained on the basis of a different concrete quality.

3.2. Steel reinforcing bars

To ascertain the nature of steel reinforcing bars, a fragment derived from the sample 24 has been investigated by optical spectrometer (Table 2). As expected, the sample resulted a carbon steel with a ferritic–pearlitic microstructure, commonly used for reinforced concrete. It should be noted that the percentage of phosphorus was close to the limit permitted by the standard (0.055% according to the UNI ENV 10080 (CEN, 2005)), while sulfur content was significantly higher than the threshold value (0.055% according same standard). The employed steel was of the expected type, its quality was mediocre, but it was still good enough to fulfill structural functions.

The metallographic analysis (Fig. 4, suppl. mat.) showed, in agreement with visual examination, that the carbon ferritic–pearlitic steel suffered from corrosion phenomena. The steel parts firmly embedded in low-carbonated concrete were characterized by a thin layer of very light surface oxide. In this case, steel was not degraded. On the contrary, reinforcing bars embedded in carbonated concrete showed increasing degrees of corrosive attack, ranging from the initial stage of a diffuse corrosion, to the final formation of corrosion crevices (Hussain and Ishida, 2009; Zivica, 2003). These bars already lost a significant part of the resistant section and were not structurally reliable (samples 8 and 30) (Fig. 4c, suppl. mat.).

In the present case, deicing salts could be occasionally present in winter, but the situation of concurrent chlorides, oxygen and water or moisture is verified only for limited periods of time. In addition, the presence of these salts might be found mainly at the base of the columns of the eastern façade, due to a great car and pedestrian traffic. However, spalling at the base of the columns was not found. Finally, in all steel bars giving rise to spalling, the corrosion morphology was always generalized, and localized pitting corrosion, typical of chloride attack, was never found. To conclude, XRD and thermal analyses (TG-DTA) confirmed the absence of chloride compounds, and the chlorides attack can be ruled out.

In all the examined samples, the reinforcements resulted totally repairable by removing the surface oxide layer, except for the sample 8, 30 and 31, which were deeply corroded (layers of rust 3–4 mm thick) and required replacement.

3.3. Facing bricks

The total open porosity of modern bricks fired between 900 and 1000 °C varies from 25 to 35% and the pore mean size between 0.5 and 1.4 μm, depending on the used clays, the firing temperature and the molding process (Cultrone et al., 2004; Rodriguez-Navarro and Doehne, 1999). Samples 16 and 19 showed a total accessible porosity respectively equal to 24.5 and 31.4% with a mean pore radius respectively of 0.63 and 1.25 μm. The presence of pores smaller than 1.5 μm may negatively affect bricks durability (Winslow et al., 1988) due to the dynamics of the water circulation within the pore structure and the generation of high crystallization pressures associated to soluble salts and freeze–thaw cycles. In both cases, crystallization pressure is inversely proportional to the pore radius (Cultrone et al., 2004; Winslow et al., 1988).

XRD analysis on samples 19 and 16 (Fig. 5, suppl. mat.) revealed the presence of quartz (Q), calcium feldspar (anorthite, albite) (F) and mica (M), which are typical constituents of bricks. The analysis conducted on sample 16 (with black crust) showed the presence of calcite (CC) and of gypsum (G). XRD analysis carried out on efflorescences over bricks of the northern side (sample 3) and of the western side (sample 17) showed the presence of magnesium sulphates (epsomite, $MgSO_4{\cdot}7H_2O$, hexahydrite, $MgSO_4{\cdot}6H_2O$ and kieserite, $MgSO_4{\cdot}H_2O$), calcium sulphate (gypsum) and sodium sulphate (thenardite, Na_2SO_4) (Fig. 5, suppl. mat.). In the sample 3, konyaite ($Na_2Mg(SO_4)_2{\cdot}5H_2O$) was also detected. TG-DTA on efflorescences from sample 3 indicated the presence of epsomite and of hexahydrite dehydrating between 20 and 210 °C and giving rise to kieserite which, in turn, formed anhydrous magnesium sulfate, between 210 and 310 °C. Gypsum decomposed between 100 and 140 °C in hemihydrate and between 180 and 200 °C in anhydrite (Fig. 6 suppl. mat.). The peaks were related to endothermic decomposition. These results confirmed XRD data. Due to their high water solubility and their strong volume expansion

during crystallization and the increase of their degree of hydration, both magnesium and sodium sulfates salts, along with bricks porosity and pore size distribution and the RH variations, may cause the occurrence of extended efflorescences and bricks pulverization (Rodriguez-Navarro and Doehne, 1999) (Fig. 2, suppl. mat.). SEM observations on sample 16 revealed also the presence of compact and adherent black crusts with average thickness of about 400 μm (Fig. 7 suppl. mat.).

4. Conclusions

Cracking and spalling of the reinforced concrete cover was the main cortical deterioration of the Palace of Public Works in Turin. Furthermore, corrosion of steel reinforced bars, due to aggressive environmental agents, was not uniform. In some large regions steel did not present any corrosion, while in other areas degradation was particularly pronounced because of the concrete poor quality and of the presence of air pollutants and localized humidity, that promoted concrete carbonation and rebar's corrosion. Regarding facing bricks and brick laying mortar, the most diffuse degradations were lacunas, pulverization, delamination, cracking, presence of efflorescences, patina and black crusts, dissolution and leaching of mortar between brick courses and the presence of salts inside the masonry. The building was finally restored in 2005 (Bono et al., 2008). The cortical concrete layer was removed exposing the reinforcements, then rebars were cleaned, protected and integrated. The section was reconstructed with shrinkage compensated mortar mixed up with metal fibers. Eight years after repairing, the new cortical layers of this building show a good state of conservation.

Appendix A. Supplementary data

Supplementary data associated with this article can be found, in the online version, at doi:10.1016/j.cscm.2014.04.006.

References

Bono D, Doglione R, Macchiorlatti-Vignat B, Pagliolico SL, Pistone G, Tulliani JM. Intervento di manutenzione straordinaria dell'edificio L.L P. P. del comune di Torino sito in piazza San Giovanni. In: Ientile R, editor. Architetture in cemento armato. Orientamenti per la conservazione, Collana Ex Fabrica. Milano: Franco Angeli; 2008. p. 81–7.

CEN, EN 10080 – Steel for the reinforcement of concrete – Weldable reinforcing steel – General. Brussels: Central Secretariat; 2005.

Cultrone G, Eduardo S, Elert K, De la Torre MJ, Cazalla O, Rodriguez-Navarro C. Influence of mineralogy and firing temperature on the porosity of bricks. J Eur Ceram Soc 2004;24:547–64.

Diamond S. Mercury porosimetry an inappropriate method for the measurement of pore size distributions in cement-based materials. Cem Concr Res 2000;30:1517–25.

EN 1992-1-1:2004 Eurocode 2: Design of concrete structures – Part 1-1: General rules and rules for buildings.

Gajda J, MacGregor Miller F. Concrete as a sink for atmospheric carbon dioxide: a literature review and estimation of CO_2 absorption by portland cement concrete, PCA R&D Serial No. 2255. Skokie, IL: Portland Cement Association; 2000.

Guemmadi Z, Resheidat M, Houari H, Toumi B. Optimal criteria of Algerian blended cement using limestone fines. J Civ Eng Manag 2008;14(4):269–75.

Ho DWS, Lewis RK. Carbonation of concrete and its prediction. Cem Concr Res 1987;17(3):489–504.

Hussain RR, Ishida T. Critical carbonation depth for initiation of steel corrosion in fully carbonated concrete and development of electrochemical carbonation induced corrosion model. Int J Electrochem Sci 2009;4:1178–95.

Lagerblad B. Numerical calculation of CO_2 uptake. In: Carbon dioxide uptake during concrete life cycle, state of the art, CBI report 2. 2005;24–8.

Pade C, Guimaraes M. The CO_2 uptake of concrete in a 100 year perspective. Cem Concr Res 2007;37:1348–56.

Rodriguez-Navarro C, Doehne E. Salt weathering: influence of evaporation rate, supersaturation and crystallization pattern. Earth Surf Process Landforms 1999;24:191–209.

UNI EN 206-1:2006 Concrete - Part 1: Specification, performance, production and conformity.

Voglis N, Kakali G, Chaniotakis E, Tsivilis S. Portland limestone cements, their properties and hydration compared to those of other composite cement. Cem Concr Compos 2005;27:191–6.

Winslow DN, Kilgour CL, Crooks RW. Predicting the durability of bricks. J Test Eval 1988;16(6):527–31.

Ye G, Lura P, van Breugel K. Modelling of water permeability in cementitious materials. Mater Struct 2006;39:877–85.

Yoon IS, Copuroglu O, Park KB. Effect of global climatic change on carbonation progress of concrete. Atmos Environ 2007;41:7274–85.

Zivica V. Corrosion of reinforcement induced by environment containing chloride and carbon dioxide. Bull Mater Sci 2003;26(6):605–8.